THE FASEB JOURNAL • RESEARCH • www.fasebj.org

In vivo imaging of prodromal hippocampus CA1 subfield oxidative stress in models of Alzheimer disease and Angelman syndrome

Bruce A. Berkowitz,[*,†,1] Jacob Lenning,[*,2] Nikita Khetarpal,[*,2] Catherine Tran,[*,2] Johnny Y. Wu,[*] Ali M. Berri,[*] Kristin Dernay,[*] E. Mark Haacke,[‡] Fatema Shafie-Khorassani,[§] Robert H. Podolsky,[§] John C. Gant,[¶] Shaniya Maimaiti,[¶] Olivier Thibault,[¶] Geoffrey G. Murphy,[‖] Brian M. Bennett,[#] and Robin Roberts[*]

[*]Department of Anatomy and Cell Biology and [†]Department of Ophthalmology, Wayne State University School of Medicine, Detroit, Michigan, USA; [‡]Department of Radiology and [§]Department of Family Medicine and Public Health Sciences, Wayne State University, Detroit, Michigan, USA; [¶]Department of Pharmacology and Nutritional Sciences, University of Kentucky Medical Center, Lexington, Kentucky, USA; [‖]Department of Molecular and Integrative Physiology, Molecular Behavioral Neuroscience Institute, University of Michigan Medical School, Ann Arbor, Michigan, USA; and [#]Centre for Neuroscience Studies, Department of Biomedical and Molecular Sciences, Faculty of Health Sciences, Queen's University, Kingston, Ontario, Canada

ABSTRACT: Hippocampus oxidative stress is considered pathogenic in neurodegenerative diseases, such as Alzheimer disease (AD), and in neurodevelopmental disorders, such as Angelman syndrome (AS). Yet clinical benefits of antioxidant treatment for these diseases remain unclear because conventional imaging methods are unable to guide management of therapies in specific hippocampus subfields *in vivo* that underlie abnormal behavior. Excessive production of paramagnetic free radicals in nonhippocampus brain tissue can be measured *in vivo* as a greater-than-normal $1/T_1$ that is quenchable with antioxidant as measured by quench-assisted (Quest) MRI. Here, we further test this approach in phantoms, and we present proof-of-concept data in models of AD-like and AS hippocampus oxidative stress that also exhibit impaired spatial learning and memory. AD-like models showed an abnormal gradient along the CA1 dorsal–ventral axis of excessive free radical production as measured by Quest MRI, and redox-sensitive calcium dysregulation as measured by manganese-enhanced MRI and electrophysiology. In the AS model, abnormally high free radical levels were observed in dorsal and ventral CA1. Quest MRI is a promising *in vivo* paradigm for bridging brain subfield oxidative stress and behavior in animal models and in human patients to better manage antioxidant therapy in devastating neurodegenerative and neurodevelopmental diseases.—Berkowitz, B. A., Lenning, J., Khetarpal, N., Tran, C., Wu, J. Y., Berri, A. M., Dernay, K., Haacke, E. M., Shafie-Khorassani, F., Podolsky, R. H., Gant, J. C., Maimaiti, S., Thibault, O., Murphy, G. G., Bennett, B. M., Roberts, R. *In vivo* imaging of prodromal hippocampus CA1 subfield oxidative stress in models of Alzheimer disease and Angelman syndrome. FASEB J. 31, 4179–4186 (2017). www.fasebj.org

KEY WORDS: reactive oxygen species · MRI · dorsoventral CA1 · neurodegenerative disease · neurodevelopment disorders

In neurodegenerative diseases, such as Alzheimer disease (AD), and in neurodevelopmental disorders, such as Angelman syndrome (AS), patients demonstrate impairment in goal location based on surrounding landmarks (*i.e.*, allocentric spatial disorientation) as one of many debilitating morbidities (1, 2). An essential brain region involved in encoding spatial memories is the CA1 subfield of the mid- and posterior hippocampus (human) or dorsal CA1 (CA1d) in rodents (3, 4). A leading hypothesis in the field based on *ex vivo* measurements is that hippocampus oxidative stress plays a pathogenic role in spatial disorientation (2, 5–16). This hypothesis has developed on the basis of studies in postmortem tissue of oxidative damage biomarkers, such as buildup of the polyunsaturated fatty acid oxidation product 4-hydroxynonenal (HNE) (17, 18). At present, it is not possible to measure excessive production of free radicals from hippocampus CA1 subfields *in vivo*. Thus, translation of basic science findings into personalized management of antioxidant treatments in patients has been limited and a major problem for clinically testing and improving therapeutic efficacy.

ABBREVIATIONS: ACSF, artificial cerebrospinal fluid; AD, Alzheimer disease; AHP, afterhyperpolarization; ALA, α-lipoic acid; AS, Angelman syndrome; CA1d, dorsal hippocampus CA1; CA1i, intermediate hippocampus CA1; HNE, 4-hydroxynonenal; LTCC, L-type calcium channel; MB, methylene blue; MEMRI, manganese-enhanced MRI; Quest MRI, quench-assisted MRI; SOD, superoxide dismutase; T_R, repetition time; 2-D, 2-dimensional; WT, wild type

[1] Correspondence: Department of Anatomy and Cell Biology, Wayne State University School of Medicine, 540 E. Canfield, Detroit, MI 48201, USA. E-mail: baberko@med.wayne.edu

[2] These authors contributed equally to this work.

doi: 10.1096/fj.201700229R

Quench-assisted (Quest) MRI has recently been suggested as a robust and sensitive tool for mapping excessive free radical production in different layers of the retina *in vivo* without a contrast agent (15, 19). The Quest MRI index of abnormally high production of paramagnetic free radicals is a greater-than-normal spin-lattice relaxation rate R_1 ($1/T_1$) that can be returned to baseline after acute antioxidant administration (15, 19, 20). Our preliminary studies find agreement between Quest MRI *in vivo* and reference standard free radical measurements in several animal models (15, 19). For example, in a mouse model of diabetic retinopathy, and in pharmaceutical and genetic models of outer retinal degeneration, Quest MRI, histochemical stains such as dichlorofluorescein and dihydroethidine, and a bioluminescence method such as lucigenin, all identify the outer retina as the first location to show evidence of oxidative stress before overt histopathology is apparent (15, 19, 21, 22). However, more work is needed in phantoms to directly confirm that sustained free radical production *per se* is what Quest MRI detects. Also, it is unclear whether Quest MRI can be applied to study nonretinal brain tissue, such as hippocampal CA1 subfields.

In this study, we tested the feasibility of using Quest MRI to provide evidence of localized oxidative stress *in vivo* in brain subfields identified from previous *ex vivo* studies in animal models that exhibit spatial disorientation. We evaluated Quest MRI during sustained superoxide production from the xanthine/xanthine oxidase reaction (23, 24). We provide proof-of-concept data that Quest MRI can be applied to evaluate hippocampus subfields *in vivo* in 3 disease models: aldehyde dehydrogenase 2-knockout mice, 5xFAD mice, and *UBE3A*-knockout mice (25–29). Aldehyde dehydrogenase 2 mice are also called HNE mice because they exhibit a greater-than-normal hippocampus concentration of the peroxidation product HNE (the earliest evidence for oxidative stress in patients with prodromal AD (30), together with spatial learning and memory impairments and age-dependent spontaneous AD-like histopathology (17). 5xFAD mice are a common β-amyloidogenic model of familial AD that demonstrates hippocampus oxidative stress (including HNE accumulation) and spatial cognitive defects (26, 28). *UBE3A*-knockout mice are a model of AS, a genetic neurodevelopmental disorder characterized by hippocampus oxidative stress and impaired goal location based on external cues and other endophenotypes consistent with that in patients with AS (2, 31). Because oxidative stress impairs L-type calcium channel (LTCC) function and afterhyperpolarization (AHP; due to reduced calcium entry) (32–36), we also examined 5xFAD mice for downstream functional oxidative damage produced by excessive free radical production. LTCC function was measured *in vivo* along the dorsal–ventral CA1 axis using manganese-enhanced MRI (MEMRI) (37); calcium-dependent AHP in the dorsal hippocampus CA1 subfield was also evaluated (35, 36).

MATERIALS AND METHODS

All animals were treated in accordance with the *Guide for the Care and Use of Laboratory Animals* (National Institutes of Health (Bethesda, MD, USA), the *Statement for the Use of Animals in Ophthalmic and Vision Research* (Association for Research in Vision and Ophthalmology, Rockville, MD, USA), and the Institutional Animal and Care Use Committee authorization (Wayne State University, University of Michigan, and the University of Kentucky). Animals were housed and maintained in 12:12-h light–dark cycle laboratory lighting, unless otherwise noted.

Experiments

In vitro study

Xanthine/xanthine oxidase is a commonly used system to continuously generate superoxide free radicals *in vitro* (23, 38). Phantoms used for this study consisted of a 0.7-ml microcentrifuge tube containing either xanthine oxidase (0.135 U/ml, 150 μl) or xanthine oxidase (0.135 U/ml, 150 μl) with either superoxide dismutase (SOD; 125 U/ml, 60 μl) or additional PBS (60 μl). After collecting baseline scans, xanthine (2.9 mM, 300 μl) was carefully added to the reaction vessel inside the magnet *via* PE20 tubing, and $1/T_1$ measurements were obtained. Preliminary experiments were performed to confirm continuous production of free radicals over the examination period based on absorbance spectroscopy (data not shown). All reagents were purchased from Sigma-Aldrich (St. Louis, MO, USA), and all stock solutions were prepared in PBS.

Animal models

Three-month-old HNE mice (17), 2-mo-old 5xFAD mice, and 4-mo-old AS mice [all on C57BL/6 (B6) backgrounds] were studied; additional age-matched B6 mice were purchased as needed (The Jackson Laboratory, Bar Harbor, ME, USA). In all cases, a baseline T_1 data set was collected and mice were allowed to recover from the isoflurane anesthesia. Thirty minutes after recovery, mice were treated with 1 mg/kg methylene blue (MB, i.p., dissolved in saline); MB is an alternate electron transporter that effectively suppresses superoxide generation from a variety of sources (39). The next day, ~1 h before the second MRI examination, each MB-treated mouse was treated with 50 mg/kg α-lipoic acid (ALA, i.p., dissolved in saline and pH adjusted to ~7.4). ALA is a potent free radical neutralizer (15, 19, 40). Mice were then reanesthetized with isoflurane, and another T_1 data set was obtained from the same brain slice. All mice were humanely killed after the second MRI examination. Some of the same 5xFAD mice were allowed to recover and were then studied by electrophysiology. A different set of 6-mo-old 5xFAD mice and age-matched controls were separately studied using MEMRI.

MRI

The general mouse preparation for high resolution 2-dimensional (2-D) MRI is well established in our laboratory (15, 19, 41). HNE, 5xFAD, and AS mice were anesthetized with isoflurane (3% induction, 1.2% maintenance) to allow for recovery. 5xFAD mice studied using MEMRI were anesthetized with urethane (36% solution i.p.; 0.083 ml/20 g animal weight, prepared fresh daily; Sigma-Aldrich). MEMRI examination of 5xFAD mice required a prior bolus injection of $MnCl_2$ (66 mg $MnCl_2{\cdot}4H_2O$/kg, i.p.) on the right side of awake mice (42). Four hours after this injection, mice were anesthetized and T_1 data obtained. In terminal studies, mice were humanely euthanized as detailed in our Division of Laboratory Animal Resources-approved protocol.

High-resolution T_1 2-D data sets were acquired on a 7 T system (Bruker ClinScan; Bruker Daltonics, Bremen, Germany). For the brain studies, a receive-only 4-element phased array coil was used. In all cases, several spin-echo images were collected (single transverse slice, echo time (T_E) 11 ms, 12 × 12 mm^2, matrix size

192 × 192, slice thickness 400 μm, turbofactor 4). For the phantom studies, a receive-only surface coil (1.0 cm diameter) was used, and 3 baseline T_1 data sets were first collected, followed by 5 additional T_1 data sets after in-magnet addition of xanthine starting at 2 min 40 s after injection, and then at 4 min 30 s, 7 min 20 s, 10 min 20 s, and 15 min 20 s after injection.

Because the Quest MRI experiment is looking for differences in $1/T_1$ between baseline and antioxidant treatment, generating a precise measure of $1/T_1$ is the major requirement. Thus, any sequence that produces precise $1/T_1$ measurements can be used for Quest MRI. Here, we performed a commonly used reference standard saturation recovery approach in which multiple repetition times (T_Rs) are used to precisely measure $1/T_1$ over a large range of signal-to-noise conditions, a procedure routinely performed in our laboratory (42–46). Images with different T_Rs were acquired in the following order (number of averages in parentheses): T_R 0.15 s (6), 3.50 s (1), 1.00 s (2), 1.90 s (1), 0.35 s (4), 2.70 s (1), 0.25 s (5), and 0.50 s (3). To compensate for reduced signal-to-noise ratios at shorter T_Rs, progressively more images were collected as the T_R decreased. The time investment is about 45 min per mouse: ~15 min to initially anesthetize the mouse, gently position it in the cradle, and center it in the magnet; 10 min to autoshim and autocoil calibrate; and ~15 min to acquire the full T_1 data set. Removing the mouse from the magnet, humanely killing the animal, and cleanup takes an additional ~5 min.

Hippocampal electrophysiology (AHP)

5xFAD mice that were examined by Quest MRI were then used for electrophysiologic characterization of the CA1d AHP. Hippocampal slices from mice were prepared as previously described in detail (47, 48). Rostral portions of freshly dissected brain hemispheres (including the hippocampus) were cut (350 μm) sequentially using a 3000 Vibratome (Thermo Fisher Scientific, Waltham, MA, USA) in oxygenated low-Ca^{2+} artificial cerebrospinal fluid (ACSF, 0.1 mM Ca^{2+}). Slices containing dorsal hippocampus were then placed in an interface-type chamber and maintained in oxygenated regular ACSF at 32°C for at least 2 h. Regular ACSF contains the following (mM): NaCl (128), KCl (3), CaCl (2), MgCl (2), glucose (10), KH_2PO_4 (1.25), and $NaHCO_3$ (26). Individual slices were transferred one at a time to a microscope stage (E600 FN; Nikon, Tokyo, Japan) equipped with a recording chamber continuously perfused (2 ml/min) with oxygenated ACSF maintained at ~32°C (TC2Bip; Cell Micro Controls, Norfolk, VA, USA). Sharp electrodes (70–90 MΩ) were used to monitor membrane voltages recorded from CA1 pyramidal neurons using an Axoclamp 2B amplifier (Molecular Devices, Sunnyvale, CA, USA). Electrodes were filled with 2 M potassium methyl sulfate ($KMeSO_4$) and 10 mM HEPES, pH 7.4, and were pulled from borosilicate glass capillaries (World Precision Instruments, Sarasota, FL, USA) on a P80 pipette puller (Sutter Instrument, Novato, CA, USA). Responses were acquired in current clamp mode and data digitized (5 kHz) and stored to PCs using pClamp 8 (Molecular Devices). To generate intracellular AHPs, neurons were held at −65 mV, and a 100 ms current depolarization pulse was delivered through the electrode to generate 4 Na^+ action potentials. AHP amplitudes were measured at the negative peak immediately following the depolarization pulse, during the medium AHP, which typically lasts several 100 ms in hippocampal pyramidal neurons, and at 800 ms after the end of the step, during the slow AHP. For each cell recorded, 4–10 depolarizations were averaged to quantify the AHP. Only neurons with input resistances >35 MΩ and overshooting action potentials (>0 mV) were included in the analysis.

MRI data analysis

Within each T_1 data set of 23 images, images acquired with the same T_R were first registered (rigid body) and then averaged to generate a stack of 8 images. These averaged images were then registered across T_Rs. The $1/T_1$ maps were then calculated *via* fitting to a 3-parameter T_1 equation $\{y = a + b \times [\exp(-c \times T_R)]$, where *a, b,* and *c* are fitted parameters$\}$ on a pixel-by-pixel basis using R v.2.9.0 software (R Foundation for Statistical Computing, Vienna, Austria; *http://www.r-project.org/*) and scripts developed in house.

Initial reports of Quest MRI normalized experimental data to same-day control mice data to minimize day-to-day variations. While effective, the approach is clearly impractical in a clinical setting and in certain experimental models. Here, we introduce new analysis procedure to eliminate the need for normalizing to same-day control mice data. Because of slice bias in the 2-D data and low signal-to-noise ratio, the T_1 estimate is highly dependent on the signal intensity of the T_R 150-ms image and thus imprecise (44). By normalizing to the shorter T_R, some of the bias can be removed giving a more accurate estimate for T_1. We normalized within and between groups for signal intensity differences by first applying 3 × 3 gaussian smoothing, performed 3 times, only on the T_R 150-ms image to minimize noise and emphasize signal. The smoothed T_R 150-ms image was then divided into the rest of the images in that T_1 data set. Preliminary experiments (data not shown) found that this procedure minimized the day-to-day variation in the $1/T_1$ profile previously noted, abrogating the need for normalization to a same-day group of control mice (15, 19).

In the brain studies, line regions of interest over presumptive CA1d spanning ~12.5 pixels (~780 μm) along the pyramidal region starting just ventral of the subiculum as assessed from the anatomic image, and a region ventral to CA1d called intermediate hippocampus CA1 (CA1i) spanning ~15.5 pixels (~969 μm) approximately midway down the pyramidal region) were identified. Average $1/T_1$ MRI data from left and right CA1d and CA1i were analyzed (15, 19).

Statistical analysis

In the phantom studies, we used a generalized estimating equation approach to examine differences between groups while appropriately accounting for correlations over time. We used a first-order autoregressive correlation structure, with similar results obtained using an unstructured correlation matrix.

In the brain studies using Quest MRI, we only examined CA1d and CA1i, conducting analyses separately for each region. By limiting the number of brain regions analyzed, we substantially improved the power of hypothesis testing using the methods presented here. While the data for each experimental strain (*i.e.,* HNE, AS, and 5xFAD) were obtained on different dates with a different set of B6 controls, we used a linear mixed model to jointly analyze all data to improve power to detect differences. The dependent variable for these analyses was $1/T_1$, and we included the following independent variables: animal strain (B6, HNE, AS, 5xFAD), MB-ALA antioxidant treatment, and the interaction between strain and MB-ALA antioxidant treatment. A random effect of mouse within strain was included to account for measuring mice before and after MB-ALA antioxidant treatment. A random effect of batch was evaluated, but this effect was not significant using a likelihood ratio test, and both Akaike's information criterion and the Schwarz Bayesian information criterion indicated that the batch random effect did not improve the fit of the models. As such, we did not include this random effect in our analyses. We initially evaluated the statistical significance of the interaction between strain and MB-ALA antioxidant treatment, and we only examined simple effects if the interaction was significant. For the test of the interaction, we used a type I error rate of 0.1 because power is often much lower for interactions. We used the resulting mixed effects model to estimate the MB-ALA antioxidant treatment effect within each

strain, the strain differences at baseline, and the strain differences under MB-ALA antioxidant treatment. Two-tailed unpaired Student *t* tests were performed on MEMRI data in each region (CA1d or CA1i), and to look for AHP differences across transgenic and wild-type (WT) animals. Data are presented as means ± SEM.

RESULTS

Detection of sustained production of free radicals by Quest MRI *in vitro*

Superoxide free radicals inside the magnet were generated using a commonly used xanthine/xanthine oxidase enzymatic system (24). This resulted in a steady ~6% increase over baseline $1/T_1$ values (**Fig. 1**). SOD added to the reaction vessel prevented the increase in $1/T_1$ (24). These results directly confirmed that continuous production of biologically relevant free radicals are readily detectable using Quest MRI.

Control mice demonstrated no evidence for changes in hippocampus CA1 $1/T_1$ *in vivo* with or without antioxidants

Comparing all control B6 mice with and without MB-ALA antioxidant treatment revealed no differences in $1/T_1$ for both CA1d (95% confidence interval, baseline: 0.65–0.68 s^{-1} and with antioxidants: 0.65–0.69 s^{-1}) and CA1i (95% confidence interval, baseline: 0.61–0.65 s^{-1} and with antioxidants: 0.62–0.66 s^{-1}).

Hippocampus CA1 excessive free radical production measured *in vivo* in HNE, AD-like, and AS models

At baseline, HNE, 5xFAD, and AS mice all had CA1d $1/T_1$ that was greater than their respective age-matched WT B6 mice (**Fig. 2**). After MB-ALA antioxidant administration, $1/T_1$ CA1d in all experimental groups were significantly reduced to WT levels. The $1/T_1$ of CA1i region in HNE or 5xFAD mice was not different from controls, whereas in the AS mice CA1i $1/T_1$ was supernormal and quenchable (Fig. 2).

Hippocampus CA1 calcium dysregulation identified *in vivo* in models of AD

In separate group of 5xFAD mice, a lower-than-normal uptake of manganese was noted in CA1d but not CA1i as measured by MEMRI (**Fig. 3**) (37, 49–51). We also found subnormal CA1d calcium-dependent AHP (Fig. 3).

DISCUSSION

The results of the present xanthine/xanthine oxidase experiment validate a key assumption of Quest MRI: sustained production of free radicals has a net detectable impact as an effective paramagnetic $1/T_1$ contrast mechanism in the absence of a spin trap contrast agent and

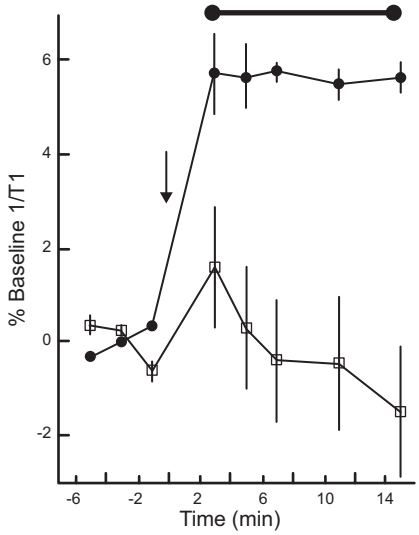

Figure 1. Detection of sustained production of free radicals by Quest MRI *in vitro*. Time course of $1/T_1$ from phantoms containing xanthine oxidase (black circles, $n = 3$) before (left of arrow, baseline) and after (right of arrow) in-magnet addition of xanthine (arrow), or containing xanthine oxidase and SOD (open squares, $n = 3$). Horizontal bar indicates significant difference range; error bars ± SEM.

potentially confounding variables that are present *in vivo* (15, 19, 20, 52, 53). It is commonly thought that because free radicals have very short lifetimes and low concentrations *in vivo*, they would have a negligible impact on water $1/T_1$ (20, 52, 54–58). However, oxidative stress is a condition that is defined as a sustained, net production of free radicals, and the available data clearly demonstrate robust detection *via* Quest MRI under these conditions (15, 19, 20, 53). Because all species of free radicals are paramagnetic, Quest MRI likely detects the total excessive free radical burden of the tissue (15, 19, 52, 53). We estimate that the xanthine oxidase generated an approximate steady state concentration of superoxide free radicals of ~60 μM. This concentration estimate is somewhat uncertain because of, for example, potential differences in viscosity between water and the intracellular environment *in vivo*, which is expected to increase free radical relaxivity (59) and the variable level of superoxide produced that depends in part on the oxygen content of the solution and enzymatic activity of a particular batch of xanthine oxidase (23, 38, 60). Unfortunately, conversion of $1/T_1$ to a superoxide concentration is also problematic because the relaxivity of superoxide radicals is not known. Intriguingly, isolated neutrophils produce an estimated total concentration of superoxide of ~76 μM, although whether this is representative of the concentration of free radicals under oxidative stress conditions *in vivo* is, to our knowledge, unknown (61). Nonetheless, the above considerations suggest that Quest MRI has sufficient sensitivity to detect an oxidative stress condition *in vivo* that produces a sustained free radical level of ~60 μM. On the basis of the data in Fig. 1, it seems likely that lower concentration levels can be detected

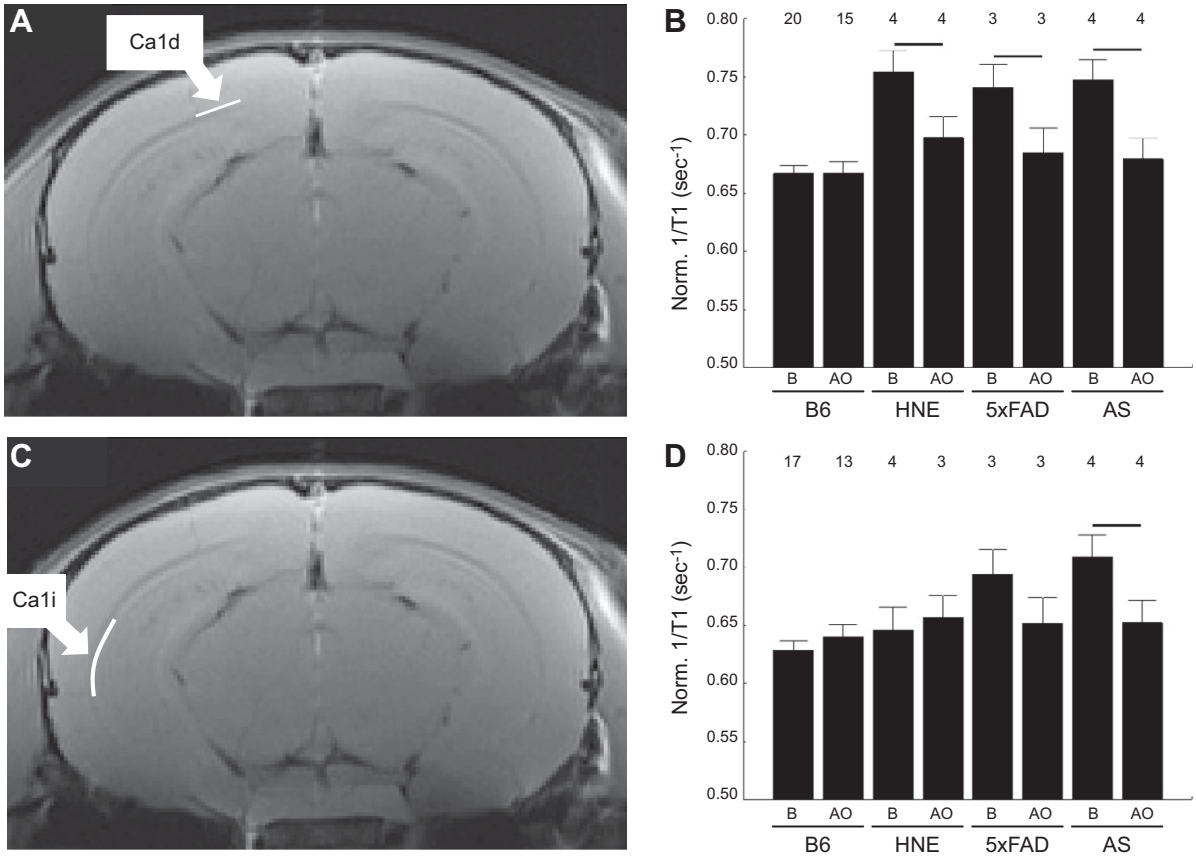

Figure 2. Hippocampus CA1 subfields demonstrates disease-dependent excessive production of free radicals *in vivo*. Representative anatomic image illustrating position of CA1d (*A*) and CA1i (*C*) regions (white lines), and corresponding bar graph summaries (*B*, *D*). Summary of normalized $1/T_1$ at baseline (*B*) and after treatment with antioxidants (AO) in B6 WT, HNE, 5xFAD, and AS mice. Numbers above bars indicate numbers of mice; error bars ± SEM; horizontal bar represents significant difference.

and more work is needed to define the detection sensitivity of Quest MRI *in vivo*.

In this study, the use of isoflurane is a potentially confounding factor because it is thought to have antioxidant effects in and of itself (62–67). This claim is somewhat controversial, however, with other studies showing a prooxidant effect of isoflurane (62–67). The experiments performed herein were not designed to resolve this conflict. Nonetheless, we note that if isoflurane exerted a major anti- or pro-oxidant action, we would expect baseline

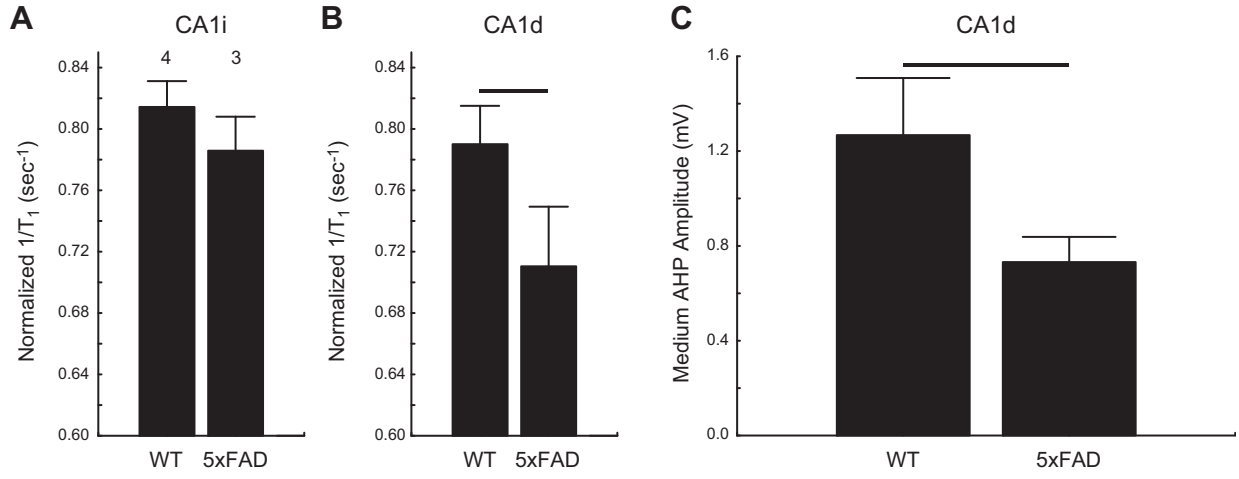

Figure 3. Hippocampus CA1d but not CA1i exhibits impaired LTCC function *in vivo*, and CA1d shows AHP reductions in 5xFAD mice compared to WT counterpart. *A*, *B*) Summary of normalized MEMRI $1/T_1$ (see Materials and Methods) of CA1i (*A*) and CA1d (*B*) in B6 WT and 5xFAD mice. Numbers above bars indicate numbers of mice; error bars = SEM. *C*) Bar graph of mean medium AHP amplitudes from CA1d neurons of WT ($n = 10$ cells from 4 mice) and 5xFAD ($n = 12$ cells from 5 mice). Horizontal bar denotes significant difference.

values between control and experimental CA1d and CA1i to be similar. However, this was not observed. Instead, we see some groups in which baseline CA1i values are similar in control and experimental mice (AD-like mice) or elevated compared to controls (AS mice). Thus, we reason that non-isoflurane-based endogenous differences in free radical production in CA1 subregions between controls and experimental mice are the dominant source of sustained free radical production observed.

CA1d and CA1i were examined herein in 3 models that have previously been shown to have hippocampus oxidative damage based on conventional *ex vivo* methods. Two spatially close hippocampal regions, CA1d and CA1i, were examined. These two regions are functionally distinct (4, 68). For example, they encode for different types of memories [*i.e.*, spatial (CA1d) *vs.* emotional (CA1i)] (3, 4, 69); they respond differently to ischemia–reperfusion (*i.e.*, CA1d exhibits 9-fold more ischemic necrosis than CA1i) (70); they have ~10% different total vascular areas (*i.e.*, CA1d < CA1i) (71); and they experience different levels of excitability (*i.e.*, CA1d < CA1i) (72). Thus, the results herein are first-time evidence supporting Quest MRI for detecting *in vivo* disease-dependent production of abnormally high levels of free radicals in CA1 subfields.

Supernormal production of free radicals is a necessary but not sufficient condition of oxidative stress (15, 19). In addition, it is helpful to provide evidence not just of oxidative stress but also of downstream oxidative damage to related physiology, such as neuronal calcium homeostasis or excitability (32–34, 48). To this end, 5xFAD mice were examined using MEMRI, the imaging modality of choice for measuring neuronal LTCC function *in vivo* (37, 49–51, 73), and by electrophysiology (35, 36). LTCCs are a cellular redox sensor (74). The combined findings of a net supernormal free radical production in CA1d compared to CA1i (Quest MRI, Fig. 2), impaired LTCC function in CA1d relative to CA1i (Fig. 3), and reduced calcium-dependent AHP in CA1d (Fig. 3) supports the presence of oxidative stress in CA1d relative to CA1i in the 5xFAD mice. The results of this study are also in line with our previous results that found agreement between outer retinal oxidative stress as measured by conventional methods and Quest MRI (15, 19).

Quest MRI offers advantages compared to other imaging methods that report on oxidative stress *in vivo* (52, 55, 57, 75–79). These other methods involve exogenously administered contrast agents that bind to free radicals (spin traps) and/or require highly specialized equipment (e.g., ref. 52). Thus, their potential clinical application is likely limited because, for example, of a combination of lack of U.S. Food and Drug Administration approval for the contrast agent, difficulty of the contrast agent crossing blood–brain/retina barriers, concerns about how disease may alter contrast agent pharmacokinetics, and possible modifications to endogenous neuronal redox signaling due to binding of free radicals (55, 57, 75–80). However, Quest MRI does not require injection of a contrast agent or require specialized equipment, and Food and Drug Administration–approved antioxidants can be used for the confirmatory quench. Thus, Quest MRI clearly has high potential for translating promising experimental treatments into clinical practice to help manage the pathogenic oxidative stress aspect of devastating neurodegenerative diseases in individual patients.

CONCLUSIONS

Localized overabundance of free radicals leading to regional oxidative stress is one of the earliest abnormalities in neurodegenerative diseases, including AD, and in neurodevelopmental disorders such as AS (2, 5–16, 21, 81–84). However, conventional imaging biomarkers cannot noninvasively measure region excess in free radical production *in vivo*. For the first time, we show in 3 different models proof of concept that Quest MRI is a promising method to address this major long-standing problem. Quest MRI has high translational potential and the potential for personalized detection over time of supernormal production of free radicals/antioxidant treatment efficacy in localized regions of the brain *in vivo*. In addition, Quest MRI appears to be useful for measuring *in vivo* brain region-specific biomarkers of the earliest relevant dysfunction underlying abnormal behaviors. FJ

ACKNOWLEDGMENTS

This work was supported, in part, by the U.S. National Institutes of Health (NIH)/National Eye Institute (NEI) (Grants R21EY021619 and R01EY026584 to B.A.B.), NIH/National Institute on Aging (Grants R01 AG033649 to O.T. and R01 AG028488 to G.G.M.), Alzheimer's Society Research Program (B.M.B.), the Canadian Vascular Network (B.M.B.), University of Michigan Protein Folding Disease Initiative (G.G.M.), NIH/NEI Core Grant P30 EY04068, and an unrestricted grant from Research to Prevent Blindness (Kresge Eye Institute, Detroit, MI, USA).

AUTHOR CONTRIBUTIONS

B. A. Berkowitz, O. Thibault, G. G. Murphy, and B. M. Bennett designed research; R. Roberts, J. Lenning, N. Khetarpal, C. Tran, A. M. Berri, K. Dernay, J. C. Gant, and S. Maimaiti performed research; B. A. Berkowitz and R. H. Podolsky, O. Thibault analyzed data; E. M. Haacke, F. Shafie-Khorassani, and R. H. Podolsky contributed new statistical analysis tools; B. A. Berkowitz, O. Thibault, G. G. Murphy, B. M. Bennett, R. Roberts, J. Lenning, N. Khetarpal, C. Tran, A. M. Berri, and R. H. Podolsky wrote the article; and J. Y. Wu developed software necessary to analyze the data.

REFERENCES

1. Vlček, K., and Laczó, J. (2014) Neural correlates of spatial navigation changes in mild cognitive impairment and Alzheimer's disease. *Front. Behav. Neurosci.* **8**, 89
2. Santini, E., Turner, K. L., Ramaraj, A. B., Murphy, M. P., Klann, E., and Kaphzan, H. (2015) Mitochondrial superoxide contributes to hippocampal synaptic dysfunction and memory deficits in Angelman syndrome model mice. *J. Neurosci.* **35**, 16213–16220
3. Moser, E., Moser, M. B., and Andersen, P. (1993) Spatial learning impairment parallels the magnitude of dorsal hippocampal lesions,

but is hardly present following ventral lesions. *J. Neurosci.* **13**, 3916–3925
4. Strange, B. A., Witter, M. P., Lein, E. S., and Moser, E. I. (2014) Functional organization of the hippocampal longitudinal axis. *Nat. Rev. Neurosci.* **15**, 655–669
5. Butterfield, D. A., Reed, T., Perluigi, M., De Marco, C., Coccia, R., Cini, C., and Sultana, R. (2006) Elevated protein-bound levels of the lipid peroxidation product, 4-hydroxy-2-nonenal, in brain from persons with mild cognitive impairment. *Neurosci. Lett.* **397**, 170–173
6. Nunomura, A., Tamaoki, T., Motohashi, N., Nakamura, M., McKeel, D. W., Jr., Tabaton, M., Lee, H. G., Smith, M. A., Perry, G., and Zhu, X. (2012) The earliest stage of cognitive impairment in transition from normal aging to Alzheimer disease is marked by prominent RNA oxidation in vulnerable neurons. *J. Neuropathol. Exp. Neurol.* **71**, 233–241
7. Shimohama, S., Tanino, H., Kawakami, N., Okamura, N., Kodama, H., Yamaguchi, T., Hayakawa, T., Nunomura, A., Chiba, S., Perry, G., Smith, M. A., and Fujimoto, S. (2000) Activation of NADPH oxidase in Alzheimer's disease brains. *Biochem. Biophys. Res. Commun.* **273**, 5–9
8. Nunomura, A., Perry, G., Aliev, G., Hirai, K., Takeda, A., Balraj, E. K., Jones, P. K., Ghanbari, H., Wataya, T., Shimohama, S., Chiba, S., Atwood, C. S., Petersen, R. B., and Smith, M. A. (2001) Oxidative damage is the earliest event in Alzheimer disease. *J. Neuropathol. Exp. Neurol.* **60**, 759–767
9. Arimon, M., Takeda, S., Post, K. L., Svirsky, S., Hyman, B. T., and Berezovska, O. (2015) Oxidative stress and lipid peroxidation are upstream of amyloid pathology. *Neurobiol. Dis.* **84**, 109–119
10. Praticò, D., Uryu, K., Leight, S., Trojanoswki, J. Q., and Lee, V. M. (2001) Increased lipid peroxidation precedes amyloid plaque formation in an animal model of Alzheimer amyloidosis. *J. Neurosci.* **21**, 4183–4187
11. McManus, M. J., Murphy, M. P., and Franklin, J. L. (2011) The mitochondria-targeted antioxidant MitoQ prevents loss of spatial memory retention and early neuropathology in a transgenic mouse model of Alzheimer's disease. *J. Neurosci.* **31**, 15703–15715
12. Massaad, C. A., Washington, T. M., Pautler, R. G., and Klann, E. (2009) Overexpression of SOD-2 reduces hippocampal superoxide and prevents memory deficits in a mouse model of Alzheimer's disease. *Proc. Natl. Acad. Sci. USA* **106**, 13576–13581
13. Kanamaru, T., Kamimura, N., Yokota, T., Iuchi, K., Nishimaki, K., Takami, S., Akashiba, H., Shitaka, Y., Katsura, K., Kimura, K., and Ohta, S. (2015) Oxidative stress accelerates amyloid deposition and memory impairment in a double-transgenic mouse model of Alzheimer's disease. *Neurosci. Lett.* **587**, 126–131
14. Chen, L., Na, R., and Ran, Q. (2014) Enhanced defense against mitochondrial hydrogen peroxide attenuates age-associated cognition decline. *Neurobiol. Aging* **35**, 2552–2561
15. Berkowitz, B. A., Bredell, B. X., Davis, C., Samardzija, M., Grimm, C., and Roberts, R. (2015) Measuring *in vivo* free radical production by the outer retina. *Invest. Ophthalmol. Vis. Sci.* **56**, 7931–7938
16. Surmeier, D. J., Guzman, J. N., Sanchez-Padilla, J., and Goldberg, J. A. (2011) The origins of oxidant stress in Parkinson's disease and therapeutic strategies. *Antioxid. Redox Signal.* **14**, 1289–1301
17. D'Souza, Y., Elharram, A., Soon-Shiong, R., Andrew, R. D., and Bennett, B. M. (2015) Characterization of Aldh2(−/−) mice as an age-related model of cognitive impairment and Alzheimer's disease. *Mol. Brain* **8**, 27
18. Hardas, S. S., Sultana, R., Clark, A. M., Beckett, T. L., Szweda, L. I., Murphy, M. P., and Butterfield, D. A. (2013) Oxidative modification of lipoic acid by HNE in Alzheimer disease brain. *Redox Biol.* **1**, 80–85
19. Berkowitz, B. A., Lewin, A. S., Biswal, M. R., Bredell, B. X., Davis, C., and Roberts, R. (2016) MRI of retinal free radical production with laminar resolution *in vivo*. *Invest. Ophthalmol. Vis. Sci.* **57**, 577–585
20. Stinnett, G., Moore, K., Samuel, E., Loic, G., Graham, B., Tour, J., and Pautler, R. G. (2015) A novel assay for the *in vivo* detection of reactive oxygen species using MRI. *ISMRM Meeting Abstracts*, 1917
21. Du, Y., Veenstra, A., Palczewski, K., and Kern, T. S. (2013) Photoreceptor cells are major contributors to diabetes-induced oxidative stress and local inflammation in the retina. *Proc. Natl. Acad. Sci. USA* **110**, 16586–16591
22. Berkowitz, B. A., Wen, X., Thoreson, W. B., Kern, T. S., and Roberts, R. (2015) Abnormal rod calcium homeostasis and the development of retinal oxidative stress in diabetes. *Invest. Ophthalmol. Vis. Sci.* **56**, 4280
23. Fridovich, I. (1970) Quantitative aspects of the production of superoxide anion radical by milk xanthine oxidase. *J. Biol. Chem.* **245**, 4053–4057
24. Suzuki, Y. J., Tsuchiya, M., and Packer, L. (1991) Thioctic acid and dihydrolipoic acid are novel antioxidants which interact with reactive oxygen species. *Free Radic. Res. Commun.* **15**, 255–263
25. D'Souza, Y., Dowlatshahi, S., and Bennett, B. M. (2011) Changes in aldehyde dehydrogenase 2 expression in rat blood vessels during glyceryl trinitrate tolerance development and reversal. *Br. J. Pharmacol.* **164**(2b), 632–643
26. Griñán-Ferré, C., Sarroca, S., Ivanova, A., Puigoriol-Illamola, D., Aguado, F., Camins, A., Sanfeliu, C., and Pallàs, M. (2016) Epigenetic mechanisms underlying cognitive impairment and Alzheimer disease hallmarks in 5XFAD mice. *Aging (Albany NY)* **8**, 664–684
27. Modi, K. K., Roy, A., Brahmachari, S., Rangasamy, S. B., and Pahan, K. (2015) Cinnamon and its metabolite sodium benzoate attenuate the activation of p21rac and protect memory and learning in an animal model of Alzheimer's disease. *PLoS One* **10**, e0130398
28. Lin, B., Hasegawa, Y., Takane, K., Koibuchi, N., Cao, C., and Kim-Mitsuyama, S. (2016) High-fat-diet intake enhances cerebral amyloid angiopathy and cognitive impairment in a mouse model of Alzheimer's disease, independently of metabolic disorders. *J. Am. Heart Assoc.* **5**, e003154
29. Wang, Q., Xiao, B., Cui, S., Song, H., Qian, Y., Dong, L., An, H., Cui, Y., Zhang, W., He, Y., Zhang, J., Yang, J., Zhang, F., Hu, G., Gong, X., Yan, Z., Zheng, Y., and Wang, X. (2014) Triptolide treatment reduces Alzheimer's disease (AD)-like pathology through inhibition of BACE1 in a transgenic mouse model of AD. *Dis. Model. Mech.* **7**, 1385–1395
30. Di Domenico, F., Tramutola, A., and Butterfield, D. A. (2016) Role of 4-hydroxy-2-nonenal (HNE) in the pathogenesis of alzheimer disease and other selected age-related neurodegenerative disorders. [Epub ahead of print] *Free Radic. Biol. Med.* doi: 10.1016/j.freeradbiomed.2016.10.490
31. Van Woerden, G. M., Harris, K. D., Hojjati, M. R., Gustin, R. M., Qiu, S., de Avila Freire, R., Jiang, Y. H., Elgersma, Y., and Weeber, E. J. (2007) Rescue of neurological deficits in a mouse model for Angelman syndrome by reduction of alphaCaMKII inhibitory phosphorylation. *Nat. Neurosci.* **10**, 280–282
32. Görlach, A., Bertram, K., Hudecova, S., and Krizanova, O. (2015) Calcium and ROS: a mutual interplay. *Redox Biology* **6**, 260–271
33. Tamagnini, F., Scullion, S., Brown, J. T., and Randall, A. D. (2015) Intrinsic excitability changes induced by acute treatment of hippocampal CA1 pyramidal neurons with exogenous amyloid β peptide. *Hippocampus* **25**, 786–797
34. Yang, L., Xu, J., Minobe, E., Yu, L., Feng, R., Kameyama, A., Yazawa, K., and Kameyama, M. (2013) Mechanisms underlying the modulation of L-type Ca^{2+} channel by hydrogen peroxide in guinea pig ventricular myocytes. *J. Physiol. Sci.* **63**, 419–426
35. Pancani, T., Anderson, K. L., Brewer, L. D., Kadish, I., DeMoll, C., Landfield, P. W., Blalock, E. M., Porter, N. M., and Thibault, O. (2013) Effect of high-fat diet on metabolic indices, cognition, and neuronal physiology in aging F344 rats. *Neurobiol. Aging* **34**, 1977–1987
36. Blalock, E. M., Phelps, J. T., Pancani, T., Searcy, J. L., Anderson, K. L., Gant, J. C., Popovic, J., Avdiushko, M. G., Cohen, D. A., Chen, K-C., Porter, N. M., and Thibault, O. (2010) Effects of long-term pioglitazone treatment on peripheral and central markers of aging. *PLoS One* **5**, e10405
37. Bissig, D., and Berkowitz, B. A. (2014) Testing the calcium hypothesis of aging in the rat hippocampus *in vivo* using manganese-enhanced MRI. *Neurobiol. Aging* **35**, 1453–1458
38. Kelley, E. E., Khoo, N. K. H., Hundley, N. J., Malik, U. Z., Freeman, B. A., and Tarpey, M. M. (2010) Hydrogen peroxide is the major oxidant product of xanthine oxidase. *Free Radic. Biol. Med.* **48**, 493–498
39. Wen, Y., Li, W., Poteet, E. C., Xie, L., Tan, C., Yan, L. J., Ju, X., Liu, R., Qian, H., Marvin, M. A., Goldberg, M. S., She, H., Mao, Z., Simpkins, J. W., and Yang, S. H. (2011) Alternative mitochondrial electron transfer as a novel strategy for neuroprotection. *J. Biol. Chem.* **286**, 16504–16515
40. Gomes, M. B., and Negrato, C. A. (2014) Alpha-lipoic acid as a pleiotropic compound with potential therapeutic use in diabetes and other chronic diseases. *Diabetol. Metab. Syndr.* **6**, 80
41. Berkowitz, B. A., Bissig, D., Patel, P., Bhatia, A., and Roberts, R. (2012) Acute systemic 11-*cis*-retinal intervention improves abnormal outer retinal ion channel closure in diabetic mice. *Mol. Vis.* **18**, 372–376
42. Berkowitz, B. A., Bissig, D., and Roberts, R. (2016) MRI of rod cell compartment-specific function in disease and treatment *in vivo*. *Prog. Retin. Eye Res.* **51**, 90–106
43. Freeman, R., and Hill, H. D. W. (1971) Fourier transform study of NMR spin-lattice relaxation of "progressive saturation." *J. Chem. Phys.* **54**, 3367–3377
44. Haacke, E. M., Brown, R. W., Thompson, M. R., and Venkatesan, R. (1999) *Magnetic Resonance Imaging: Physical Principles and Sequence Design*. Wiley, Hoboken, NJ, USA

45. Décorps, M., Laval, M., Confort, S., and Chaillout, J. J. (1985) Signal to noise and spatial localization of NMR spectra with a surface coil and the saturation–recovery sequence. *J. Magn. Reson.* **61**, 418–425
46. Hsu, J. J., Glover, G. H., and Zaharchuk, G. (2009) Optimizing saturation–recovery measurements of the longitudinal relaxation rate under time constraints. *Magn. Reson. Med.* **62**, 1202–1210
47. Thibault, O., and Landfield, P. W. (1996) Increase in single L-type calcium channels in hippocampal neurons during aging. *Science* **272**, 1017–1020
48. Thibault, O., Pancani, T., Landfield, P. W., and Norris, C. M. (2012) Reduction in neuronal L-type calcium channel activity in a double knock-in mouse model of Alzheimer's disease. *Biochim. Biophys. Acta* **1822**, 546–549
49. Bissig, D., and Berkowitz, B. A. (2011) Same-session functional assessment of rat retina and brain with manganese-enhanced MRI. *Neuroimage* **58**, 749–760
50. Bissig, D., and Berkowitz, B. A. (2009) Manganese-enhanced MRI of layer-specific activity in the visual cortex from awake and free-moving rats. *Neuroimage* **44**, 627–635
51. Holt, A. G., Bissig, D., Mirza, N., Rajah, G., and Berkowitz, B. (2010) Evidence of key tinnitus-related brain regions documented by a unique combination of manganese-enhanced MRI and acoustic startle reflex testing. *PLoS One* **5**, e14260
52. Hyodo, F., Murugesan, R., Matsumoto, K., Hyodo, E., Subramanian, S., Mitchell, J. B., and Krishna, M. C. (2008) Monitoring redox-sensitive paramagnetic contrast agent by EPRI, OMRI and MRI. *J. Magn. Reson.* **190**, 105–112
53. Bakalova, R., Georgieva, E., Ivanova, D., Zhelev, Z., Aoki, I., and Saga, T. (2015) Magnetic resonance imaging of mitochondrial dysfunction and metabolic activity, accompanied by overproduction of superoxide. *ACS Chem. Neurosci.* **6**, 1922–1929
54. Beeman, S. C., Shui, Y.-B., Perez-Torres, C. J., Engelbach, J. A., Ackerman, J. J. H., and Garbow, J. R. (2016) O_2-sensitive MRI distinguishes brain tumor versus radiation necrosis in murine models. *Magn. Reson. Med.* **75**, 2442–2447
55. Zhelev, Z., Bakalova, R., Aoki, I., Lazarova, D., and Saga, T. (2013) Imaging of superoxide generation in the dopaminergic area of the brain in Parkinson's disease, using mito-TEMPO. *ACS Chem. Neurosci.* **4**, 1439–1445
56. Hyodo, F., Chuang, K. H., Goloshevsky, A. G., Sulima, A., Griffiths, G. L., Mitchell, J. B., Koretsky, A. P., and Krishna, M. C. (2008) Brain redox imaging using blood–brain barrier–permeable nitroxide MRI contrast agent. *J. Cereb. Blood Flow Metab.* **28**, 1165–1174
57. Towner, R. A., Smith, N., Saunders, D., Henderson, M., Downum, K., Lupu, F., Silasi-Mansat, R., Ramirez, D. C., Gomez-Mejiba, S. E., Bonini, M. G., Ehrenshaft, M., and Mason, R. P. (2012) *In vivo* imaging of immuno-spin trapped radicals with molecular magnetic resonance imaging in a diabetic mouse model. *Diabetes* **61**, 2405–2413
58. Mason, R. P. (2016) Imaging free radicals in organelles, cells, tissue, and *in vivo* with immuno-spin trapping. *Redox Biol.* **8**, 422–429
59. Bennett, H. F., Brown III, R. D., Koenig, S. H., and Swartz, H. M. (1987) Effects of nitroxides on the magnetic field and temperature dependence of $1/T_1$ of solvent water protons. *Magn. Reson. Med.* **4**, 93–111
60. Kuppusamy, P., and Zweier, J. L. (1989) Characterization of free radical generation by xanthine oxidase. Evidence for hydroxyl radical generation. *J. Biol. Chem.* **264**, 9880–9884
61. Ilangovan, G., Zweier, J. L., and Kuppusamy, P. (2004) Microximetry: simultaneous determination of oxygen consumption and free radical production using electron paramagnetic resonance spectroscopy. *Methods in Enzymology* **381**, 747–762
62. Rocha, T. L. A., Dias-Junior, C. A., Possomato-Vieira, J. S., Goncalves-Rizzi, V. H., Nogueira, F.R.,de Souza, K.M., Braz, L. G., and Braz, M. G. (2015) Sevoflurane induces DNA damage whereas isoflurane leads to higher antioxidative status in anesthetized rats. *BioMed Res. Int.* **2015**, 264971
63. Schallner, N., Ulbrich, F., Engelstaedter, H., Biermann, J., Auwaerter, V., Loop, T., and Goebel, U. (2014) Isoflurane but not sevoflurane or desflurane aggravates injury to neurons *in vitro* and *in vivo via* p75NTR-NF-κB activation. *Anesth. Analg.* **119**, 1429–1441
64. Crystal, G. J., Malik, G., Yoon, S. H., and Kim, S. J. (2012) Isoflurane late preconditioning against myocardial stunning is associated with enhanced antioxidant defenses. *Acta Anaesthesiol. Scand.* **56**, 39–47
65. Hu, Q., Ma, Q., Zhan, Y., He, Z., Tang, J., Zhou, C., and Zhang, J. (2011) Isoflurane enhanced hemorrhagic transformation by impairing antioxidant enzymes in hyperglycemic MCAO rats. *Stroke* **42**, 1750–1756
66. Durak, I., Oztürk, H. S., Dikmen, B., Güven, C., Cimen, M. Y., Büyükkoçak, S., Kaçmaz, M., and Avci, A. (1999) Isoflurane impairs antioxidant defence system in guinea pig kidney. *Can. J. Anaesth.* **46**, 797–802
67. Kudo, M., Aono, M., Lee, Y., Massey, G., Pearlstein, R. D., and Warner, D. S. (2001) Absence of direct antioxidant effects from volatile anesthetics in primary mixed neuronal–glial cultures. *Anesthesiology* **94**, 303–312
68. Fanselow, M. S., and Dong, H.-W. (2010) Are the dorsal and ventral hippocampus functionally distinct structures? *Neuron* **65**, 7–19
69. Yiu, A. P., Rashid, A. J., and Josselyn, S. A. (2011) Increasing CREB function in the CA1 region of dorsal hippocampus rescues the spatial memory deficits in a mouse model of Alzheimer's disease. *Neuropsychopharmacology* **36**, 2169–2186
70. Ashton, D., Van Reempts, J., Haseldonckx, M., and Willems, R. (1989) Dorsal–ventral gradient in vulnerability of CA1 hippocampus to ischemia: a combined histological and electrophysiological study. *Brain Res.* **487**, 368–372
71. Grivas, I., Michaloudi, H., Batzios, Ch., Chiotelli, M., Papatheodoropoulos, C., Kostopoulos, G., and Papadopoulos, G. C. (2003) Vascular network of the rat hippocampus is not homogeneous along the septotemporal axis. *Brain Res.* **971**, 245–249
72. Malik, R., Dougherty, K. A., Parikh, K., Byrne, C., and Johnston, D. (2016) Mapping the electrophysiological and morphological properties of CA1 pyramidal neurons along the longitudinal hippocampal axis. *Hippocampus* **26**, 341–361
73. Ramos de Carvalho, J. E., Verbraak, F. D., Aalders, M. C., van Noorden, C. J., and Schlingemann, R. O. (2014) Recent advances in ophthalmic molecular imaging. *Surv. Ophthalmol.* **59**, 393–413
74. Muralidharan, P., Cserne Szappanos, H., Ingley, E., and Hool, L. (2016) Evidence for redox sensing by a human cardiac calcium channel. *Sci. Rep.* **6**, 19067
75. Prunty, M. C., Aung, M. H., Hanif, A. M., Allen, R. S., Chrenek, M. A., Boatright, J. H., Thule, P. M., Kundu, K., Murthy, N., and Pardue, M. T. (2015) *In vivo* imaging of retinal oxidative stress using a reactive oxygen species–coactivated fluorescent probe. *Invest. Ophthalmol. Vis. Sci.* **56**, 5862–5870
76. Hyodo, F., Soule, B. P., Matsumoto, K., Matusmoto, S., Cook, J. A., Hyodo, E., Sowers, A. L., Krishna, M. C., and Mitchell, J. B. (2008) Assessment of tissue redox status using metabolic responsive contrast agents and magnetic resonance imaging. *J. Pharm. Pharmacol.* **60**, 1049–1060
77. Matsumura, A., Emoto, M. C., Suzuki, S., Iwahara, N., Hisahara, S., Kawamata, J., Suzuki, H., Yamauchi, A., Sato-Akaba, H., Fujii, H. G., and Shimohama, S. (2015) Evaluation of oxidative stress in the brain of a transgenic mouse model of Alzheimer disease by *in vivo* electron paramagnetic resonance imaging. *Free Radic. Biol. Med.* **85**, 165–173
78. Sarracanie, M., Armstrong, B. D., Stockmann, J., and Rosen, M. S. (2014) High speed 3D overhauser-enhanced MRI using combined b-SSFP and compressed sensing. *Magn. Reson. Med.* **71**, 735–745
79. Rayner, C. L., Bottle, S. E., Gole, G. A., Ward, M. S., and Barnett, N. L. (2016) Real-time quantification of oxidative stress and the protective effect of nitroxide antioxidants. *Neurochem. Int.* **92**, 1–12
80. Ekanger, L. A., and Allen, M. J. (2015) Overcoming the concentration-dependence of responsive probes for magnetic resonance imaging. *Metallomics* **7**, 405–421
81. Massaad, C. A., Amin, S. K., Hu, L., Mei, Y., Klann, E., and Pautler, R. G. (2010) Mitochondrial superoxide contributes to blood flow and axonal transport deficits in the Tg2576 mouse model of Alzheimer's disease. *PLoS One* **5**, e10561
82. Han, B. H., Zhou, M. L., Johnson, A. W., Singh, I., Liao, F., Vellimana, A. K., Nelson, J. W., Milner, E., Cirrito, J. R., Basak, J., Yoo, M., Dietrich, H. H., Holtzman, D. M., and Zipfel, G. J. (2015) Contribution of reactive oxygen species to cerebral amyloid angiopathy, vasomotor dysfunction, and microhemorrhage in aged Tg2576 mice. *Proc. Natl. Acad. Sci. USA* **112**, E881–E890
83. Fanelli, F., Sepe, S., D'Amelio, M., Bernardi, C., Cristiano, L., Cimini, A., Cecconi, F., Ceru', M. P., and Moreno, S. (2013) Age-dependent roles of peroxisomes in the hippocampus of a transgenic mouse model of Alzheimer's disease. *Mol. Neurodegener.* **8**, 8
84. Furman, R., Murray, I. V. J., Schall, H. E., Liu, Q., Ghiwot, Y., and Axelsen, P. H. (2016) Amyloid plaque–associated oxidative degradation of uniformly radiolabeled arachidonic acid. *ACS Chem. Neurosci.* **7**, 367–377

Received for publication March 19, 2017.
Accepted for publication May 22, 2017.